The intrinsic stability of metal ion complexes with nanoparticulate fulvic acids

The Intrinsic Stability of Metal Ion Complexes with Nanoparticulate Fulvic Acids

Raewyn M. Town[1,4*], Jérôme F. L. Duval[2,3], and Herman P. van Leeuwen[4]

[1] Systemic Physiological and Ecotoxicological Research (SPHERE), Department of Biology, University of Antwerp, Groenenborgerlaan 171, 2020 Antwerp, Belgium. Email: raewyn.town@uantwerpen.be

[2] CNRS, Laboratoire Interdisciplinaire des Environnements Continenteaux (LIEC), UMR 7360, Vandoeuvre-lès-Nancy, F-54501 Nancy, France

[3] Université de Lorraine, LIEC, UMR 7360, Vandoeuvre-lès-Nancy, F-54501 Nancy, France

[4] Physical Chemistry and Soft Matter, Wageningen University & Research, Stippeneng 4, 6708 WE Wageningen, The Netherlands

Abstract

The electrostatic contributions to metal ion binding by fulvic acids (FAs) are characterised in light of recent theoretical developments on description of the net charge density of soft nanoparticles. Under practical electrolyte concentrations, the radius of the small, highly charged soft nanoparticulate FAs is comparable to the electrostatic screening length and their electric potential profile has a bell shape that extends into the surrounding aqueous medium. Consequently, accumulation of counterions in the extraparticulate zone can be significant. By comparison of experimentally-derived Boltzmann partitioning coefficients with those computed on the basis of (i) the structural FA particle charge and (ii) the potential profile for a nanoparticulate FA entity equilibrated with indifferent electrolyte, we identify the thickness of the *extraparticulate* counter charge accumulation shell in 1-1 and 2-1 electrolytes. The results point to the involvement of counterion condensation phenomena and call into question the approaches for modelling electrostatic contributions to ion binding that are invoked by popular equilibrium speciation codes. Overall, the electrostatic contributions to Cd^{2+}_{aq} and Cu^{2+}_{aq} association with FA are weaker than those previously found for much larger humic acids

(HA). The intrinsic chemical binding strength of CdFA is comparable to that of CdHA, whilst CuFA complexes are weaker than CuHA ones.

INTRODUCTION

Humic substances (HS) are heterogeneous complexants that are ubiquitous in environmental systems and play an important role in buffering concentrations of cations and small molecules.[1] On the basis of their solubility in water, HS are separated into a larger humic acid (HA) fraction and a smaller, more soluble fulvic acid (FA) fraction. A typical FA entity has a radius of the order of 1 nm, and contains *ca*. 5 to 10 ionisable carboxyl groups and up to one N- or S- containing functionality.[1-3] In contrast, the radii of HA particles ranges from a few nm for aquatic HA up to the order of 100 nm for soil HA aggregates, with each particle containing hundreds to thousands of chemically diverse groups.[1] The smaller FA are more conformationally rigid than the larger HA.[4-6] Most literature on binding of aqueous transition metal ions M^{2+}_{aq} (M in short) by HS describes the strength of M-HS association in terms of an *apparent* stability constant, $\overline{K}_{app}$.[7,8] That is, all M associated with the HS is considered to be chemically bound and concentrations of the complex species MHS are expressed as smeared-out over the entire volume of the solution/dispersion. The overbar notation signifies that $\overline{K}_{app}$ represents a weighted average of the stabilities over all associated forms of M with HS. $\overline{K}_{app}$ values for MHA are generally significantly greater than those for MFA.[9,10]

Recent work has shown that a more differentiated approach is needed to describe ion association with HA: the extent to which *e.g.* M^{2+} associates with negative HA entities is determined by a combination of electrostatic association and inner-sphere complexation.[11,12] The electric field contribution to ion association by HA can be significant, leading some authors to propose that Ca^{2+} association has an intrinsic chemical nature.[13-15] Rather, the extent to which the predominantly electrostatically binding Ca^{2+} ion associates with large HA particles is well described by a two-state Counterion Condensation-Donnan (CCD) model that combines (i) electric condensation of Ca^{2+} in the strongly negatively charged intraparticulate double layer shell at the particle/medium interface, with (ii) Donnan partitioning in the net uncharged core of the particle body.[11] Even for metal ions such as Cd^{2+} and Cu^{2+}, whose association with HA includes substantial inner-sphere complex

formation, a significant amount of the total M associated with the HA particle can be in the form of electrostatically condensed ions in the intraparticulate part of the double-layer shell.[12] Such detail in the intraparticulate speciation is fundamental for proper interpretation of $\bar{K}_{app}$ values, metal speciation dynamics and bioavailability.

Although FAs carry a high negative charge density at near neutral pH, their small size implies that the CCD model is not an appropriate descriptor of their electrostatic features.[9,16,17] Since κr_p (ratio between particle radius r_p, and electrostatic screening length, $1/\kappa$) is typically of order unity for FA under practical electrolyte concentrations, counterion accumulation in the *extraparticulate* double layer zone may constitute a significant fraction of the associated M.[9,18,19] This feature of ion binding by FA differs significantly from that for the larger HA ($\kappa r_p >> 1$) for which the accumulation of cations in the extraparticulate double layer zone is generally insignificant with respect to that inside the bulk particle body. The present work compares the *intrinsic* stability of inner-sphere metal complexes of FA with those of HA. In doing so, we elucidate the extent to which the differences in *apparent* stability constants for MFA and MHA can be attributed to inherent physicochemical differences in the electrostatic *vs.* the intrinsic covalent components of M binding.

THEORY

Electrostatic Characteristics of FA. At near-neutral pH, an individual FA entity (r_p *ca.* 1 nm) houses approximately 5 negatively charged sites.[20] Various types of humic substances are reported to have a density in the range *ca.* 1.4 – 2 kg m^{-3} and *ca.* 80% water content.[21-23] The FA used herein has a density of 1.5 kg m^{-3},[21] which corresponds to a local, intraparticulate charge density of *ca.* -2,000 mol *e* m^{-3} (with *e* the elementary charge). For a homogeneous distribution of charged sites, the average site separation distance, ℓ_C, is approximately 1 nm, and thus the possibility arises for overlap of the electric double layers around individual charged sites. The thickness of the electric double layer, *i.e.* the Debye screening length κ^{-1}, depends on the ionic environment. For charges within a soft nanoparticle body, the relevant screening length is the local *intraparticulate* one, κ_p^{-1}.[24,25] Once $2\kappa_p^{-1}$ becomes comparable to or greater than ℓ_C, the electrostatics can be

described by a mean-field approach, whereas for $2\kappa_p^{-1} << \ell_C$, the applicable potential is dominated by the local coulombic field around each site.[16] In a 1-1 electrolyte, κ_p can be evaluated from:[24-26]

$$\kappa_p = \kappa[\cosh(y_{center})]^{1/2} \quad (1)$$

where y_{center} is the dimensionless potential at the center of the soft charged particle computed *via* the Poisson-Boltzmann mean field approach,[26] and κ is the conventional reciprocal Debye length of the *extraparticulate* medium. Thus, for FA in 1-1 electrolyte, *e.g.* KNO_3, at an ionic strength, *I*, of 10 mM, κ_p^{-1} = 0.58 nm, and at *I* = 100 mM, κ_p^{-1} = 0.39 nm. In a 2-1 electrolyte, κ_p^{-1} is obtained via (see Supporting Information):

$$\kappa_p = \frac{\kappa}{\sqrt{3}}\left[2\exp\left(-2y_{center}\right) + \exp\left(y_{center}\right)\right]^{1/2} \quad (2)$$

Application of eq 2 for the nanoparticulate FA in 2-1 electrolyte, *e.g.* $Ca(NO_3)_2$, at *I* = 10 mM, yields κ_p^{-1} = 0.26 nm, and at *I* = 100 mM, κ_p^{-1} = 0.24 nm. Thus, the FA system is poised at the point where the double layers around individual charges begin to overlap and hence continuous electrostatic models become more appropriate. The use of discrete approaches further requires arbitrary choices about the relative positions of charged sites,[27,28] which are expected to vary considerably between individual FA entities. Herein we analyse FA electrostatics with a continuous approach, and invoke discrete concepts merely for particle charge numbers and ratios. We note that the relative magnitudes of κ_p and r_p precludes the existence of a Donnan phase which requires $\kappa_p r_p >> 1$.[16,24-26]

To date, the electrostatic features of nanoparticles have been described on the basis of *structural charge* characteristics.[19,29] Recent work has presented a framework for computing the potential profile of small charged nanoparticles *equilibrated* in aqueous electrolytes, accounting for charge compensation by the indifferent electrolyte ions.[30] The following outlines the fundamental aspects of the two approaches; the outcomes are then discussed in context of experimental results for ion association with FA.

Structural Charge Features. For a random distribution of charged sites in a soft, ion-permeable spherical nanoparticulate FA body of radius r_p, the radial distribution of the electrostatic potential $\psi(r)$ generally has a bell shape that increasingly extends into the medium as the ionic strength decreases.[9,19,26] [Hereafter, r denotes the radial coordinate with $r = 0$ the particle center.] The equilibrium accumulation of M at a distance r from the center of the FA can be described by a Boltzmann partitioning coefficient, f_B, computed via the mean field Poisson-Boltzmann approach:

$$f_B(r) = \exp[-z_M \boldsymbol{U}(r)] \tag{3}$$

where $\boldsymbol{U}$ is the dimensionless electrostatic potential energy at radial distance r, *i.e.* $\boldsymbol{U} = U(r)/kT = F\psi(r)/RT$, where k, F, R, and T have their usual meanings. The extent of counterion accumulation is obtained by computing the integral Boltzmann partitioning coefficient, $\overline{f}_B^{(s)}$, over the spatial scale from the particle center to r, *i.e.*:

$$\overline{f}_B^{(s)}(r) = \left(\int_0^r 4\pi r'^2 f_B(r')\mathrm{d}r' \right) / V(r) \tag{4}$$

where r' is a dummy integration variable and $V(r) = 4\pi r^3/3$. Using eq 4, we distinguish the extent of counterion accumulation *within the FA particle body*, $\overline{f}_{B,intra}^{(s)} = \overline{f}_B^{(s)}(r = r_p)$, from that spanning over only the *extraparticulate* double layer ($r > r_p$), $\overline{f}_{B,extra}^{(s)}(r > r_p)$, *i.e.*:

$$\overline{f}_{B,extra}^{(s)}(r > r_p) = \left(\int_{r_p}^r 4\pi r'^2 f_B(r')\mathrm{d}r' \right) / \left(V(r) - V(r_p)\right) = \frac{V(r)\overline{f}_B^{(s)}(r) - V(r_p)\overline{f}_B^{(s)}(r_p)}{V(r) - V(r_p)}. \tag{5}$$

As a consequence of the particle potential profile, extraparticulate counterions are less strongly associated than those within the particle body. The $\overline{f}_B^{(s)}$ values for 2+ counterions computed *via* eq 4 for a particle with r_p of 1 nm and charge density of -2,000 mol e m^{-3} in 1-1 and 2-1 electrolytes at I = 10 and 100 mM are shown in Figure 1. It is evident that counterion accumulation in the extraparticulate zone is significant. To highlight this aspect, Figure S1 shows the ratio $\left[\overline{f}_{B,extra}^{(s)}(r) - 1\right] / \overline{f}_{B,intra}^{(s)}$ that compares counterion accumulation in the extraparticulate zone ($r > r_p$) to that within the particle body.

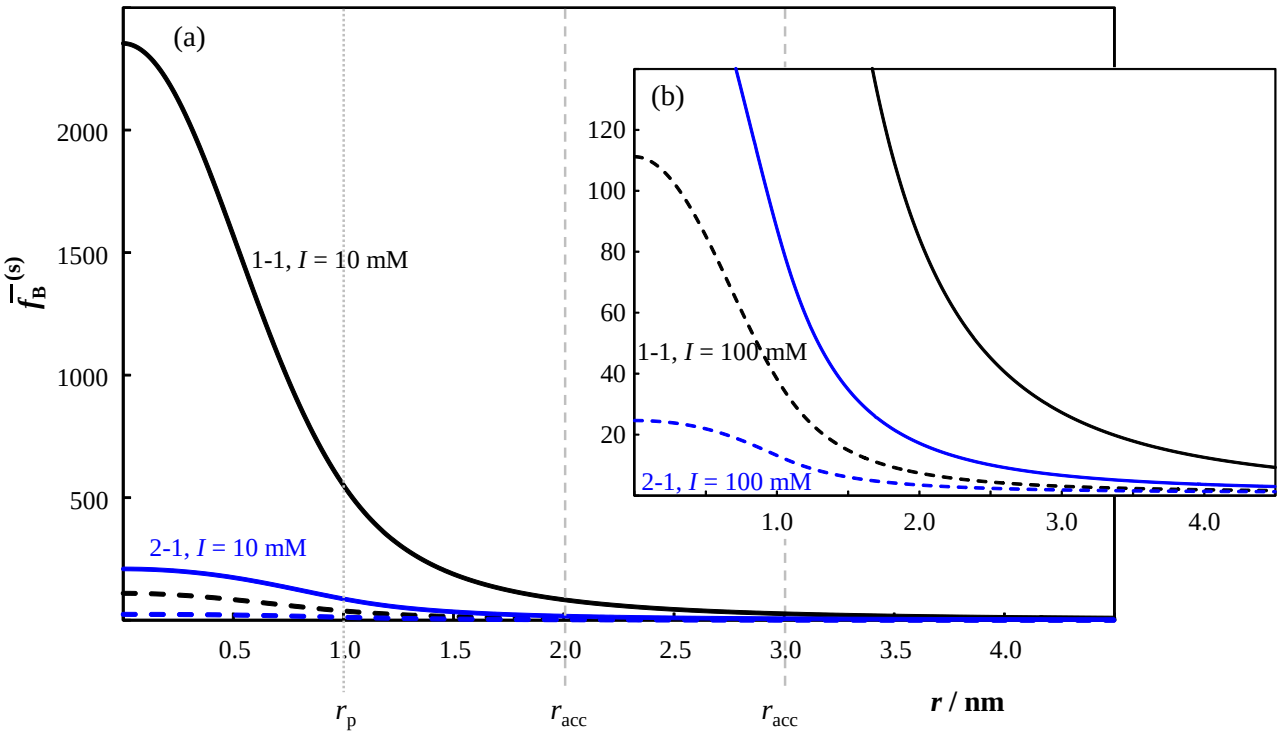

Figure 1. Structural charge-derived average Boltzmann partitioning coefficient, $\overline{f}_B^{(s)}$ (eq 4) for 2+ counterions, as a function of the radial distance, *r*, from the center of a negatively charged soft FA particle with radius, r_p, of 1 nm and structural charge density of -2,000 mol *e* m^{-3} in various bulk electrolyte media.. All data are shown in (a); the inset (b) is an amplification at small $\overline{f}_B^{(s)}$. The curves correspond to 1-1 electrolyte at *I* = 10 mM (black solid curve) and 100 mM (black dashed curve), and 2-1 electrolyte at *I* = 10 mM (blue solid curve) and 100 mM (blue dashed curve). On the *x*-axis, *r* = 0 denotes the center of the particle body and r_{acc} at 2 nm and 3 nm indicates the radii of the counterion accumulation volumes considered for interpreting data on electrostatic binding of metal ions by FA (see text for details).

The electrostatic contribution to association of M with a small charged nanoparticle generally involves both the intraparticulate and the extraparticulate electric field. For the extraparticulate component, it is necessary to determine a cut-off point, beyond which counterion accumulation is no longer significant. As arbitrary first estimates, we take cut-off points as the distance from the particle surface at which the derivative of $\overline{f}_{B,extra}^{(s)}\left(r > r_p\right)$ with respect to *r* has decreased to 10% and 2% of its value at the particle surface, $r = r_p$. This criterion locates a distance of *ca*. 1 nm and 2 nm from the particle surface, respectively. That is, counterion

accumulation is practically significant over a volume of radius *ca.* 2 to 3 nm (denoted by r_{acc} in Figures 1 and S1), comprising the FA particle body (r_p = 1 nm) plus an extraparticulate shell extending 1 or 2 nm from the particle/medium interface, practically independent of the ionic strength and electrolyte type (1-1 or 2-1) considered. This spatial scale is similar to the thickness of Manning's counterion condensation volume around linear polyionic charges (*ca.* 2 nm),[31] and the intraparticulate counterion condensation layer thickness of 2 nm found for large soft HA nanoparticles.[11,12,32]

Potential Profile at the Equilibrated FA/Medium Interface. The potential profile at the equilibrated FA/medium interface accounts for the reduction in net charge density of the FA due to accumulation of counterions within the particle body *and* the relevant extraparticulate zone.[30] For the general nanoparticle case, starting from the structural charge density, an iterative process was recently elaborated to evaluate the potential profile such that the amount of accumulated counterion charges is in equilibrium with the net particle charge.[30] Evidently, the lower the ionic strength, the greater the extent to which counterions accumulate and thus the lower the net particle charge density.[30] The Boltzmann partitioning coefficient for the equilibrated situation, $\overline{f}_B^{(eq)}(r)$, is obtained from the concentration ratio of counterions in the accumulation volume $V(r)$ and in the bulk medium.[30] Under the conditions considered herein, the concentration of the target M is orders of magnitude lower than that of the electrolyte cations, thus electrostatic partitioning of M is dictated by the electric field set by the electrolyte, *i.e.* by $\overline{f}_B^{(eq)}$.

Intrinsic Stability Constants. Measurement of the extent to which M associates with HA in indifferent 1-1 electrolyte as compared to that in 2-1 electrolyte has been established as a useful means to evaluate the electrostatic contribution to M binding.[11,12] The electrostatic contribution will be greater in an indifferent 1-1 electrolyte such as KNO_3 as compared to that in a 2-1 electrolyte such as $Ca(NO_3)_2$, with the concentration of Ca^{2+} in vast excess over that of the electrostatically similar M^{2+}. For large soil-derived HA, this approach was shown to give results consistent with the CCD electrostatic model.[32]

169 The intrinsic stability constant, $\overline{K}_{\mathrm{int}}$, represents the inherent chemical affinity between M and a binding site
170 S, *i.e.* not including electrostatic contributions beyond the atom/atom bond distance. That is:

171 $$\overline{K}_{\mathrm{int}} = c_{\mathrm{MS}} / c_{\mathrm{M}} c_{\mathrm{S}} \quad (6)$$

172 where c_{MS}, c_{M} and c_{S} are the *local* intraparticulate concentrations of inner-sphere complexes, free metal ion
173 and free reactive sites, respectively. For the chemically heterogeneous FA, the magnitude of $\overline{K}_{\mathrm{int}}$ depends on
174 the degree of site occupation, θ_{M}, of the binding sites by M.[1] We note that many equilibrium speciation codes
175 define θ_{M} as the ratio of concentrations of 'bound metal' and available reactive sites, where 'bound metal' is
176 tacitly taken as comprising all forms of M that are associated with the particle, *i.e.* including the intraparticulate
177 free ions, the outer-sphere complexes, the extraparticulate excess in the double layer and the condensed fraction
178 in the intraparticulate double layer zone. For characterising the heterogeneity of $\overline{K}_{\mathrm{int}}$ we define a true θ_{M}
179 which reflects the ratio between the concentrations of inner-sphere complexes and total reactive sites, *i.e.*:

180 $$\theta_{\mathrm{M}} = c_{\mathrm{MS}} / c_{\mathrm{S,t}} \quad (7)$$

181

182 # MATERIALS AND METHODS

183 **Reagents and Solution Conditions.** All solutions were prepared in ultrapure deionized water (resistivity
184 > 18 MΩ cm) from a Milli-Q Gradient system. Metal ion solutions were prepared by dilution of standards
185 (Aldrich). Ionic strength was maintained at 10 or 100 mM with KNO_3 or $Ca(NO_3)_2$ (BDH, AnalaR). Solutions
186 were buffered to pH 6 with 1 mM MES buffer ((2-(*N*-morpholino)ethanesulfonic acid) prepared from the solid
187 (Fluka, MicroSelect, ≥ 99.5%). A pH of 6 was chosen to prevent the formation of metal hydroxy species and/or
188 ternary M-FA-OH complexes.[33] The FA sample was Suwannee River fulvic acid from the International Humic
189 Substances Society (IHSS): it has a density of 1500 kg m^{-3},[21] a charge density of -10 meq gC^{-1} at pH 6,[20] a
190 carbon content of 52% (IHSS data sheet), a hydrated particle radius of *ca*. 1 nm,[3] and molar mass in the range
191 *ca*. 550 – 1000 g mol^{-1}.[21,34-36] In combination, these parameters yield a water content in the range 74-85% (see
192 Supporting Information for details).

193

194 **Electrochemical Measurements.** The electrochemical measurements were performed with an Ecochemie
195 μAutolab potentiostat (input impedance > 100 GΩ) coupled with a Metrohm VA stand. The working electrode

196 was a Metrohm multimode mercury drop electrode, the auxiliary electrode was glassy carbon, and the reference
197 electrode was Ag|AgCl|KCl(sat) encased in a 100 mM KNO_3 jacket. Solutions were initially purged with
198 oxygen-free N_2, and a nitrogen blanket was maintained during measurements. Total metal concentrations in
199 the range $2x10^{-4}$ to $7x10^{-3}$ mol m^{-3}, and total FA concentrations in the range 10 to 40 g m^{-3} were used to generate
200 the range of θ_M values studied. The concentration of free M in the bulk medium, c_M^*, was obtained from
201 equilibrium measurements in the foot of the stripping chronopotentiometry at scanned deposition potential
202 (SSCP) wave, which equates to the method of Absence of Gradients and Nernstian Equilibrium Stripping
203 (AGNES).[37] The heterogeneity parameter Γ was obtained from the shape of the experimental SSCP wave, as
204 described in previous work.[38,39] The oxidation step was performed under complete depletion conditions
205 (stripping current = 2 nA), which renders the signal practically free from adsorption effects.[40-42] Equilibrium
206 was rapidly attained upon mixing the metal and fulvic solutions: the SCP stripping time, τ, measured *ca*. 15
207 mins after mixing M and FA remained constant over several hours. This result is expected for the small, non-
208 aggregating Suwannee River FA,[43] at a pH below that at which metal ion hydrolysis occurs,[33] and is in line
209 with the fast ionic partition processes in charged nanoparticles (nano to microsecond scales).[17,44]
210
211 **Determination of the Electrostatic Contribution to M-FA Association.** The electrostatic contribution
212 to ion association by FA is much smaller than that for HA and thus it is difficult to measure FA association
213 parameters for predominantly electrostatically associating ions such as Ca^{2+}.[45--49] Accordingly, a strategic
214 experimental approach was adopted to gain insight into the electrostatic contribution to M association with FA
215 by conducting measurements in 1-1 and 2-1 electrolytes of different ionic strength.[11,12] At a given metal-to-
216 binding site ratio,, the difference between $\overline{K}_{app}$ values in the various electrolytes can be ascribed to differences
217 in the magnitude of the electrostatic contribution. $Ca(NO_3)_2$ at I = 100 mM was taken as the 'reference' medium
218 with insignificant electrostatic binding of target M, *i.e.* $\overline{f}_B$ = 1. Experimentally-derived $\overline{f}_B$ values are
219 obtained from the ratio of $\overline{K}_{app}$ in a given electrolyte to that in the reference electrolyte. Agreement between
220 the experimental values and the computed $\overline{f}_B^{(s)}$ and $\overline{f}_B^{(eq)}$ values is used to identify the spatial zone over which
221 counterion accumulation is significant. The $\overline{K}_{int}$ values are obtained *via* eq 6 using $c_M = \overline{f}_B c_M^*$. Further details
222 are given in the Supporting Information.

RESULTS AND DISCUSSION

Characterisation of the Electrostatic Contribution to M^{2+}-FA Association. The values of the apparent stability constant, $\overline{K}_{app}$, for CdFA and CuFA are shown in Figure 2. $\overline{K}_{app}$ is defined in terms of smeared-out concentrations, without discrimination between the intraparticulate species, i.e. $\overline{K}_{app} = \bar{c}_{M,b} / c_M^*(\bar{c}_{S,t} - \bar{c}_{M,b})$, where $\bar{c}_{M,b}$ is the smeared out concentration of all forms of M associated with the FA particle, and $\bar{c}_{S,t}$ is the smeared-out total concentration of binding sites. Binding of Cd at pH 6 and I = 100 mM in 1-1 and 2-1 electrolyte was too weak for reliable measurements to be obtained by AGNES in the $\bar{c}_{M,b} / \bar{c}_{S,t}$ range of interest. From Figure 2, the $\overline{f}_B$ value relative to that for $Ca(NO_3)_2$ at I = 100 mM, is found to be 26 for I = 10 mM KNO_3, and 5 for both KNO_3 at I = 100 mM and $Ca(NO_3)_2$ at I = 10 mM (Table 1). For both Cd(II) and Cu(II), similar electrostatic contributions are in effect: at I =10 mM the same factor difference was observed between $\overline{K}_{app}$ measured in KNO_3 and $Ca(NO_3)_2$. This observation supports the theoretical approach, *i.e.* the electrostatic contribution to M^{2+}-FA association is independent of the nature of the ion.

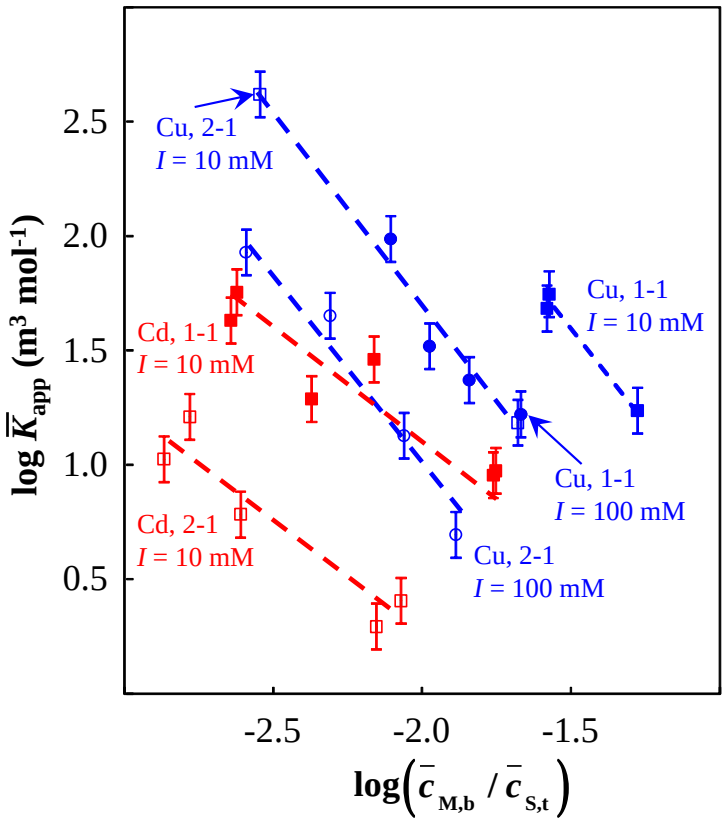

Figure 2. Apparent stability constants, $\overline{K}_{app}$, obtained *via* smeared-out concentrations for Cd(II) (red symbols) and Cu(II) (blue symbols) complexes with FA as a function of the degree of association of M with FA, $\bar{c}_{M,b} / \bar{c}_{S,t}$. Data were obtained from AGNES measurements in $Ca(NO_3)_2$ at an ionic strength of 100 mM (open circles) and 10 mM (open squares), and in KNO_3 at an ionic strength of 100 mM (solid circles), and 10 mM (solid squares). The error bars correspond to the experimental uncertainty of ± 0.1 in log $\overline{K}_{app}$. The blue dashed lines through the Cu(II) data have a slope of -1.65 and the red dashed lines through the Cd(II) data have a slope of -1. For Cu(II), the standard error on the experimental data relative to the line with slope of -1.65 is 0.22 for data measured in I = 10 mM KNO_3, 0.26 for I = 100 mM $Ca(NO_3)_2$, and 0.14 for the data measured in I = 100 mM KNO_3 and I = 10 mM $Ca(NO_3)_2$. For Cd(II), the standard error on the experimental data relative to the line with slope of -1 is 0.19 for I = 10 mM KNO_3 and 0.20 for I = 10 mM $Ca(NO_3)_2$.

Comparison of Computed and Experimental Boltzmann Partitioning Coefficients, $\overline{f}_B$. For the FA conditions, *i.e.* r_p of 1 nm and charge density -2,000 mol *e* m^{-3}, the $\overline{f}_B$ values computed on the basis of the density of structural charges, $\overline{f}_B^{(s)}$, and from the equilibrated net FA charge, $\overline{f}_B^{(eq)}$, are given in Table 1. The values depend on the thickness of the extraparticulate layer over which counterion accumulation is considered to be significant. Following the structural charged-based approach (eq 4), the $\overline{f}_B^{(s)}$ values computed for the spatial zone r = 0 to $r = r_p$ + 2 nm are in good agreement with experimental values for all electrolyte compositions considered. Despite this good agreement, the $\overline{f}_B^{(s)}$ values do not account for charge compensation by the indifferent electrolyte ions,[30] and thus the interpretation is far less rigorous than that based on the $\overline{f}_B^{(eq)}$ values. In this context it is relevant to highlight that the timescale for ionic partitioning in soft charged nanoparticles is rather fast (nano- to microsecond scale).[17,44] Thus, background electrolyte ions will rapidly attain their equilibrium distribution between the bulk medium and the particle phase, in accordance with their respective concentrations and $\overline{f}_B$ values. This feature is simply accounted for by consideration of *equilibrated* net FA charges, which shows up feasible differences in the spatial zone relevant for counterion accumulation. For 1-1 electrolyte (I = 10 and 100 mM) and 2-1 electrolyte at I = 100 mM, the $\overline{f}_B^{(eq)}$ values computed for the

spatial zone $r = 0$ to $r = r_p + 1$ nm are in best agreement with experimental data, whilst for a 2-1 electrolyte I = 10 mM the $\overline{f}_B^{(eq)}$ computed for the spatial zone $r = 0$ to $r = r_p + 2$ (or 2.5) nm yields the best agreement (Table 1). These observations can be explained by considering the number, hydration state, and charge density of the counterions. At I = 100 mM in $Ca(NO_3)_2$ the $\overline{f}_B^{(eq)}$ value corresponds to *ca*. 1 Ca^{2+} associated with each FA entity, and in 100 mM KNO_3 $\overline{f}_B^{(eq)}$ corresponds to 1.6 K^+ per FA. In both cases, electrostatically associated cations occupy the spatial zone from $r = 0$ to $r = r_p + 1$ nm. On the other hand, at the lower ionic strength of 10 mM in $Ca(NO_3)_2$ there are *ca*. 2.3 Ca^{2+} accumulated per FA, and in 10 mM KNO_3 there are 4.8 K^+ per FA, *i.e*. practically full compensation of the structural charge in both cases. The experimental results are consistent with the 4.8 K^+ occupying a spatial zone from $r = 0$ to $r = r_p + 1$ nm whilst the 2.3 Ca^{2+} occupy space from r = 0 to $r = r_p + 2$ nm (Table 1). This observation points to (a greater extent of) partial dehydration of the larger K^+ ion in the outer-sphere configuration, and is suggestive of counterion condensation. In a soft particle body such phenomena generally occur at larger ℓ_C than that needed to invoke condensation around line charges.[50] In 2-1 electrolyte at I = 10 mM, the larger accumulation zone is consistent with the greater electrostatic attraction of the 2+ ion over larger distances and the greater affinity of the 2.3 Ca^{2+} for their associated H_2O molecules: the charge density of the bare Ca^{2+} and Gibbs energy of hydration of Ca^{2+} is *ca*. 4 times greater than that of K^+.[51]

To estimate the influence of uncertainties in the values, we performed a sensitivity analysis to encompass the range of parameters applicable to Suwannee River FA, i.e. r_p = 0.8 to 1.5 nm (corresponding to extremes of the Gaussian distribution of particle sizes),[3] and charge density = -312 to -4122 mol e m^{-3} (arising from the range of reported molar masses and consequent water content; see Supporting Information). The outcomes are presented in Tables S1-S6, and the ensuing consequences for the $\overline{K}_{int}$ values computed from implementation of $\overline{f}_B^{(eq)}$ are shown in Figures S2-S5 in the Supporting Information. An analysis of the root mean squared error (RMSE) between the modelled and experimental $\overline{K}_{int}$ values confirms that the data presented in Table 1 provide the best description of the experimental data, i.e. the RMSE for these conditions is lower than that for any of the other conditions considered, where $\mathrm{RMSE} = \sqrt{\frac{1}{n}\sum_n [\log(\overline{K}_{int})_{theory} - \log(\overline{K}_{int})_{experiment}]^2}$, for the

summation over the number, *n*, of θ_M values at which $\overline{K}_{int}$ was determined for the combined Cd and Cu datasets. These RMSE values are given in the caption of Figure 3 and Figures S2-S5.

Table 1. Comparison of Computed and Experimentally-Derived Magnitudes of the Electrostatic Boltzmann Partitioning Coefficient, $\overline{f}_B$, for Divalent Cations. Values in parentheses correspond to different spatial zones of counterion accumulation. Experimental data correspond to Cd(II) and Cu(II) binding by FA.

Electrolyte and ionic strength	**Theoretical**		**Experimental**
	equilibrated charge, $\overline{f}_B^{(eq)}$	structural charge, $\overline{f}_B^{(s)}$	Figure 3[d]
KNO_3, I = 10 mM	25.79 [b] (7.42 [a])	27.21 [a] (84.37 [b])	26 (12-57)
KNO_3, I = 100 mM	1.69 [b] (NA [a])	3.06 [a] (7.38 [b])	5 (3-10)
$Ca(NO_3)_2$, I = 10 mM	9.89 [n_{Ca}=2.25] [a] (36.45 [n_{Ca}=2.46] [b]) (5.67 [n_{Ca}=2.05] [c])	6.62 [a] (17.19 [b])	5(3-10)
$Ca(NO_3)_2$, I = 100 mM	1.40 [n_{Ca}=0.94] [b] (NA [a])	1.84 [a] (3.46 [b])	1[e]

[a] integral from $r = 0$ to $r = r_p + 2$ nm, *i.e.* $\overline{f}_B^{(eq)}\left(r = r_{acc} = 3 \text{ nm}\right)$ or $\overline{f}_B^{(s)}\left(r = r_{acc} = 3 \text{ nm}\right)$

[b] integral from $r = 0$ to $r = r_p + 1$ nm, *i.e.* $\overline{f}_B^{(eq)}\left(r = r_{acc} = 2 \text{ nm}\right)$ or $\overline{f}_B^{(s)}\left(r = r_{acc} = 2 \text{ nm}\right)$

[c] integral from $r = 0$ to $r = r_p + 2.5$ nm, *i.e.* $\overline{f}_B^{(eq)}\left(r = r_{acc} = 3.5 \text{ nm}\right)$

[d] experimental $\overline{f}_B$ values are obtained from the difference between the dashed lines shown in Figure 3. The range of values in parentheses is obtained from the standard errors on the regression lines (see Figure 2 caption).

[e] reference electrolyte, for which the *a priori* $\overline{f}_B$ value of unity is supported by the corresponding theoretical $\overline{f}_B^{(eq)}$ value

n_{Ca} is the average number of Ca^{2+} per FA

NA: not applicable, because a 2 nm extension of the condensation volume from the FA surface significantly exceeds the 0.96 nm extraparticulate Debye length operational in 100 mM solution ionic strength (see ref. 30 for details)

We note that our findings are in strong contrast to the much larger electrostatic contribution to ion binding that is invoked by equilibrium speciation codes, such as WHAM[52] and NICA-Donnan.[53] For example, at I = 10 mM in 1-1 electrolyte, the NICA-Donnan model predicts, on the basis of an inappropriate Donnan potential profile, a Boltzmann partitioning coefficient of *ca*. 10^4 for FA. This picture is not physicochemically sound: the size of FA is far too small to generate a true Donnan phase within the particle body, let alone to accommodate the required massive amount of counterions. Indeed, indiscriminate implementation of Donnan volumes in equilibrium speciation codes as descriptors for electrostatic interactions between metal ions and humic substances is a generally erroneous strategy, as pointed out in our previous work.[11,12,50]

The Intrinsic and Heterogeneous Stability of Cd(II) and Cu(II) Complexes with FA. The $\overline{K}_{\mathrm{int}}$ values for FA are shown as a function of θ_{M} in Figure 3. The magnitude of $\overline{f}_{\mathrm{B}}$ corresponds to a modest contribution of electrostatics to M association with FA. For both metal ions, over the entire θ_{M} range studied, the ratio between the intraparticulate concentrations of free M and inner-sphere complexed M is well below unity. Details of the procedure used to obtain the intraparticulate concentrations and $\overline{K}_{\mathrm{int}}$ are given in the Supporting Information. As an illustrative example, for CdFA in 10 mM KNO_3 at a total Cd concentration of 4.7×10^{-3} mol m^{-3} and an FA concentration of 30 g m^{-3}, the measured free M in the bulk solution is 1.92×10^{-3} mol m^{-3}, which translates to an intraparticulate free M concentration of 5×10^{-2} mol m^{-3}, a corresponding concentration of inner-sphere complexes of 48.9 mol m^{-3} (99.9% of the intraparticulate M) and θ_{M} = 0.024. This is in strong contrast to the intraparticulate speciation found for soil HA, e.g. for CdHA at θ_{M} = 0.02, where *ca.* 40% of the particle-associated Cd was found to be in the form of inner-sphere complexes.[32] Evidently, electrostatic cooperativity is manifest to a much greater extent in the large soil HA particles with Donnan behavior and counterion condensation phenomena. Figure 3 also compares the $\overline{K}_{\mathrm{int}}$ values for FA with those reported previously for HA.[32] For the two types of HS, $\overline{K}_{\mathrm{int}}$ for Cu(II) is greater than that for Cd(II) over

the considered θ_M range. $\overline{K}_{int}$ for Cd(II) complexes is similar for FA and HA, and is comparable to that for Cd(II) complexes with simple carboxylic acids such as malonic acid.[54] In contrast, significant differences in binding behavior are observed for Cu(II). Notably, for θ_M values below *ca.* 0.03, $\overline{K}_{int}$ for CuHA is greater than that for CuFA, with the difference in magnitude increasing with decreasing θ_M, which may reflect differences in the nature of heterogeneity for the two types of HS. As typical for heterogeneous complexants, $\overline{K}_{int}$ for both FA and HA is dependent on θ_M, *i.e.* the extent to which the reactive sites are involved in inner-sphere complexation. For many types of HS the double logarithmic plot of $\overline{K}_{app}$ *vs.* θ_M is a straight line with slope equal to -1/Γ, where Γ is the heterogeneity parameter ($0 < \Gamma \leq 1$; $\Gamma = 1$ for the homogenous case).[1] The heterogeneity of metal complexes with HS generally follows the order Cu > Pb > Cd,[1,38,55] which reflects the different chemical binding features of the metal ions as elaborated in environmental context by Turner and coworkers.[56] For CdFA, our data (Figure 3) yield a Γ value close to unity, *i.e.* CdFA complexation is rather homogeneous. In contrast, Cu(II) complexation is more heterogeneous, and different behavior is found for FA as compared to HA: a Γ value of 0.6 is obtained for CuFA, *cf.* 0.2 for CuHA. For the range of θ_M values considered herein, the effective number of Cu^{2+} ions associated with an individual FA entity is less than one. Accordingly, the heterogeneity of FA is largely inter-particulate, *i.e.* the Γ value of 0.6 represents the particle-to-particle heterogeneity of individual FA entities.[57,58] For HA, the much greater number of reactive sites per individual entity means that θ_M corresponds to many metal ions associated with an individual HA, and thus Γ reflects the intra-particulate heterogeneity, *i.e.* the range of chemical functionalities within each HA entity.[59]

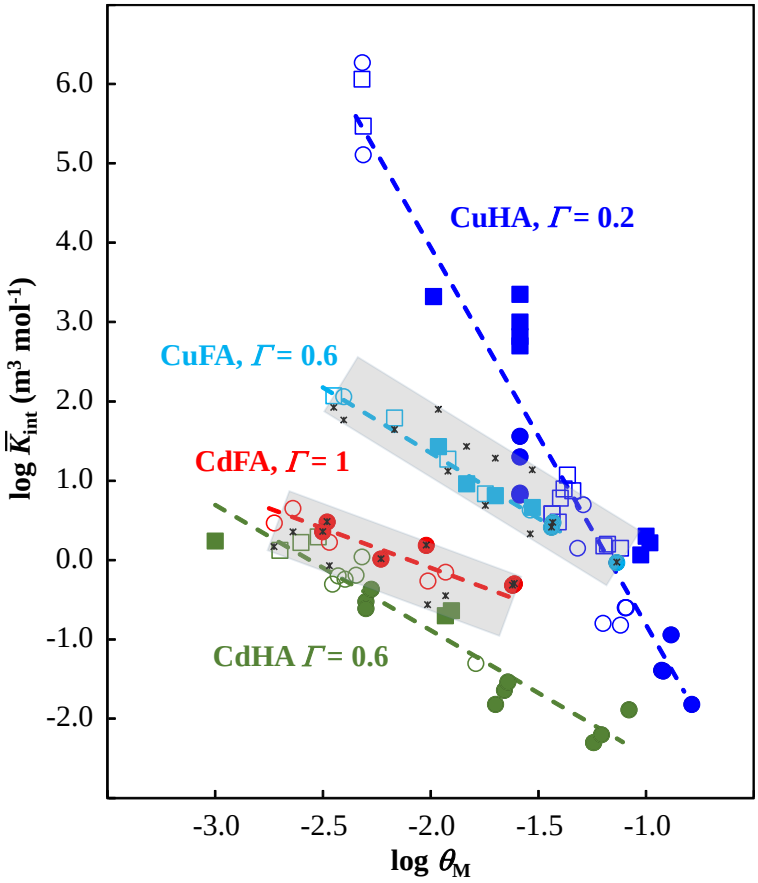

Figure 3. Comparison of the intrinsic stability constants, $\overline{K}_{int}$, determined for Cd(II) and Cu(II) complexes with fulvic acid (FA) and humic acid (HA) as a function of the degree of occupation of reactive sites by inner-sphere complexes, i.e. the true θ_M (eq 7). The coloured points for CdFA and CuFA are experimental data obtained using the experimentally derived $\overline{f}_B$ values (Table 1), a charge density of -2000 mol *e* m^{-3} and water content of 74% (see Supporting Information for details). The dashed lines have slopes of -1/Γ for each of the indicated Γ values. The standard error of the CdFA data relative to the line for Γ = 1 is 0.12, and the standard error of the CuFA data relative to the line for Γ = 0.6 is 0.07. The black asterisks correspond to the modelled values obtained using the equilibrated charge, $\overline{f}_B^{(eq)}$, values in Table 1 (the values not in parentheses in each case), and for visual convenience the shaded grey bar encompasses the range of modelled values. The RMSE between the modelled and experimental $\overline{K}_{int}$ values = 0.257 (see main text). The various symbols for the experimental data correspond to measurements at ionic strengths of 10 mM in KNO_3 (solid circles), 100 mM in KNO_3 (solid squares), 10 mM in $Ca(NO_3)_2$ (open circles) and 100 mM in $Ca(NO_3)_2$ (open squares). The different colors denote CuHA (dark blue), CuFA (light blue), CdHA (dark green), and CdFA (red). The HA

363 data are obtained from a previous publication (standard error of the CdHA data relative to the line for Γ = 0.6
364 is 0.11; standard error of the CuHA data relative to the line for Γ = 0.2 is 0.27).[32]
365
366 To further investigate the heterogeneity features of MHS binding, Γ values were also obtained from the shape
367 of experimental SSCP waves (Figure 4).[38,39] Previous work on CuHA showed excellent agreement between
368 the magnitude of Γ obtained from the slope of the log $\overline{K}_{\mathrm{int}}$ *vs.* log θ_{M} plot and that obtained from the shape
369 of an SSCP wave.[32] The consistent shape of the SSCP waves for CuHA at different θ_{M} values is shown in
370 Figure S2. For CuFA at θ_{M} = 0.03, the Γ value obtained from the slope of the log $\overline{K}_{\mathrm{int}}$ *vs.* log θ_{M} plot was the
371 same as that corresponding to the shape of the SSCP wave, but significant discrepancies were found at lower
372 θ_{M} values. For example, at θ_{M} = 0.003, the SSCP wave shape corresponded to Γ = 0.2 (Figure 4), *i.e.* CuFA
373 complexation is much more heterogeneous at very low θ_{M}, in apparent contrast with the data in Figure 3. To
374 understand this feature we need to consider the nature of the SSCP wave. Notably, on passing from the foot to
375 the plateau, there is a progressive decrease in the concentration of free M at the electrode surface, and thus also
376 in the *local* metal-to-binding site ratio.[38,39] As a consequence, increasingly more stable complexes become
377 significant in determining the flux of M towards the electrode. Nevertheless, the magnitude of the SSCP
378 *plateau* remained consistent with that predicted for the fully labile case. Thus, for a unimodal distribution of
379 CuFA entities, we would expect the shape of the SSCP wave, *i.e.* Γ, to be independent of θ_{M}. The observation
380 that the SSCP wave for CuFA is more elongated at a bulk θ_{M} of 0.003 *cf.* 0.03 (Figure 4), points to a
381 multimodal distribution: the stronger and more heterogeneous binding observed at low θ_{M} likely reflects the
382 diversity of the fewer but stronger binding sites. Potential candidates are N- and S- containing functional
383 groups. This line of reasoning is in accordance with the concept of 'major' versus 'minor' sites proposed by
384 Buffle to explain metal binding features of HS,[60,61] and the reported very low complexing capacity of the
385 strongest sites in FA.[8,62] Literature data on CuFA complexation correspond to θ_{M} values greater than *ca.* 0.003,
386 and collated $\overline{K}_{\mathrm{app}}$ *vs.* θ_{M} plots for CuFA yield a Γ value of *ca.* 0.5, in accordance with the present work.[1] This
387 outcome highlights the utility of flux based electrochemical speciation techniques, such as SSCP, which allow
388 a broad range of effective θ_{M} values to be probed for a single bulk solution composition.

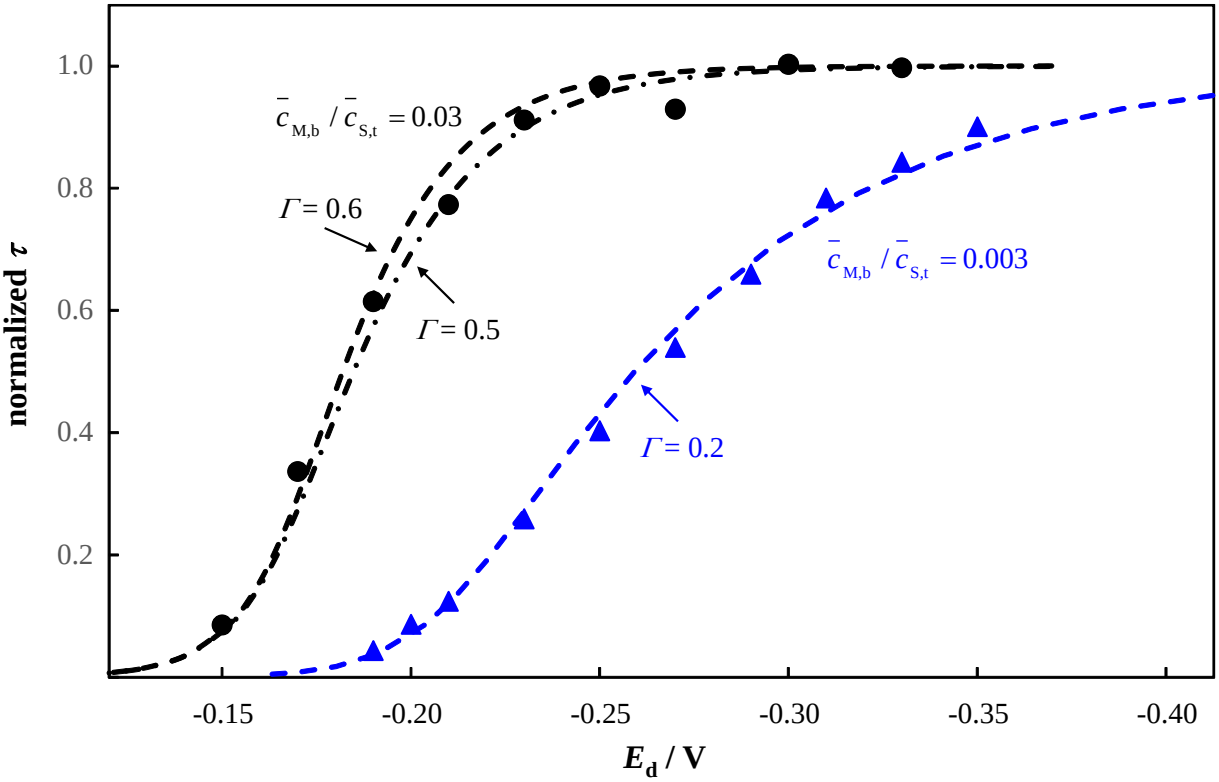

Figure 4. Experimental and computed SSCP waves (normalized reoxidation time, τ, as a function of deposition potential, E_d) for Cu(II) complexes with fulvic acid at pH 6 in $Ca(NO_3)_2$ electrolyte at I = 100 mM. Points are experimental data; dashed curves are computed for the Γ values indicated on the figure.

All in all, our strategy provides a robust means to identify the electrostatic and chemical contributions to metal ion binding by nanoparticulate FA, and thereby characterise the intrinsic heterogeneity of MFA complexes. The most rigorous description of the electrostatic contribution to M binding by small nanoparticles ($\kappa r_p \approx 1$) is obtained *via* the *equilibrated* potential profile. The extent of counterion accumulation, and the available spatial zone for that, point to the involvement of simultaneous Boltzmann partitioning and counterion condensation. The extent to which the electrostatic field contributes to M association with FA is much less significant than for HA, underscoring the reduced cooperativity in effect for small nanoparticles with dimensions of the order of the Debye screening length. These findings underscore the need for equilibrium speciation codes to incorporate dedicated electrostatic descriptors that robustly account for the size and charge density of nanoparticulate complexants such as humic substances. A detailed exploration of the implications of the present work in this context is the subject of forthcoming work. Knowledge of the intraparticulate

405 speciation is also significant for prediction of the lability and bioavailability of nanoparticulate metal species:
406 obviously, the dynamic features of the intraparticulate free M differ from those of the inner-sphere complexes.
407

408 ACKNOWLEDGEMENTS

409 RMT conducted this work within the framework of the EnviroStress Centre of Excellence at the University of
410 Antwerp.
411
412 The authors declare no competing financial interest.
413

414 ASSOCIATED CONTENT

415 **Supporting Information**

416 The Supporting Information is available free of charge on the ACS Publications website at DOI: xxx

417 The derivation of eq 2, Figure S1 showing the relative magnitude of counterion accumulation in the
418 extraparticulate zone as compared to that within the FA body, explanation of the procedures used to
419 obtain the water content and charge density of FA, and the $\overline{K}_{\mathrm{int}}$ values, Tables S1-S6 showing the
420 sensitivity analysis for the computed $\overline{f}_{\mathrm{B}}^{(\mathrm{eq})}$ and $\overline{f}_{\mathrm{B}}^{(\mathrm{s})}$ values, Figures S2-S5 showing the sensitivity
421 analysis for the $\overline{K}_{\mathrm{int}}$ values, and Figure S6 showing the SSCP waves for CuHA (PDF)

422

423 REFERENCES

(1) Buffle, J. *Complexation Reactions in Aquatic Systems: an Analytical Approach*; Ellis Horwood: Chichester, U.K., 1988.

(2) Buffle, J.; Zhang, Z.; Startchev, K. Metal flux and dynamic speciation at (bio)interfaces. Part I: Critical evaluation and compilation of physicochemical parameters for complexes with simple ligands and fulvic/humic substances. *Environ. Sci. Technol.* **2007**, *41*, 7609-7620.

(3) Lead, J. R.; Wilkinson, K. J.; Balnois, E.; Cutak, B. J.; Larive, C. K.; Assemi, S.; Beckett, R. Diffusion coefficients and polydispersities of the Suwannee River fulvic acid: comparison of fluorescence

correlation spectroscopy, pulsed-field gradient nuclear magnetic resonance, and flow field-flow fractionation. *Environ. Sci. Technol.* **2000**, *34*, 3508-3513.

(4) Lakshman, S.; Mills, R.; Fang, F.; Patterson, H.; Cronan, C. 1996. Use of fluorescence polarization to probe the structure and aluminium complexation of three molecular weight fractions of a soil fulvic acid. *Anal. Chim. Acta* **1996**, *321*, 113-119.

(5) Nebbioso, A.; Piccolo, A. Molecular rigidity and diffusivity of Al^{3+} and Ca^{2+} humates as revealed by NMR spectroscopy. *Environ. Sci. Technol.* **2009**, *43*, 2417-2424.

(6) Buffle, J.; Wilkinson, K. J.; Stoll, S.; Filella, M.; Zhang, J. A generalized description of aquatic colloidal interactions: the three-colloidal component approach. *Environ. Sci. Technol.* **1998**, *32*, 2887-2899.

(7) Buffle, J.; Deladoey, P.; Greter, F. L.; Haerdi, W. Study of the complex formaton of copper(II) by humic and fulvic substances. *Anal. Chim. Acta* **1980**, *116*, 255-274.

(8) Buffle, J.; Zhang, Z.; Startchev, K. Metal flux and dynamic speciation at (bio)interfaces. Part I: Critical evaluation and compilation of physiochemical parameters for complexes with simple ligands and fulvic/humic substances. *Environ. Sci. Technol.* **2007**, *41*, 7609-7620.

(9) Town, R. M.; H. P. van Leeuwen, H. P.; Buffle, J. Chemodynamics of soft nanoparticulate complexes: Cu(II) and Ni(II) complexes with fulvic acids and aquatic humic acids. *Environ. Sci. Technol.* **2012**, *46*, 10487-10498.

(10) Town, R. M.; Duval, J. F. L.; Buffle, J.; van Leeuwen, H. P. Chemodynamics of metal complexation by natural soft colloids: Cu(II) binding by humic acid. *J. Phys. Chem. A* **2012**, *116*, 6489-6496.

(11) Town, R. M.; van Leeuwen, H. P. Intraparticulate speciation analysis of soft nanoparticulate metal complexes. The impact of electric condensation on the binding of Cu^{2+}/Pb^{2+}/Cu^{2+} by humic acids. *Phys. Chem. Chem. Phys.* **2016**, *18*, 10049-10058.

(12) Town, R. M.; van Leeuwen, H. P. Metal ion – humic acid nanoparticle interactions: role of both complexation and condensation mechanisms. *Phys. Chem. Chem. Phys.* **2016**, *18*, 18024-18032.

(13) van den Hoop, M. A. G. T.; van Leeuwen, H. P.; Pinheiro, J. P.; Mota, A. M. Mota, Simões Gonçalves, M. L. Voltammetric analysis of the competition between calcium and heavy metal for complexation by humic material. *Coll. Surf. A: Physicochem. Eng. Aspects* **1995**, *95*, 305-313.

(14) Benedetti, M. F.; Milne, C. J.; Kinniburgh, D. G.; van Riemsdijk, W. H.; Koopal, L. K. Metal ion binding to humic substances: application of the non-ideal competitive adsorption model. *Environ. Sci. Technol.* **1995**, *29*, 446-457.

(15) Marang, L.; Eidner, S.; Kumke, M. U.; Benedetti, M.; Reiller, P. E. Spectroscopic characterization of the competitive binding of Eu(III), Ca(II), and Cu(II) to a sedimentary originated humic acid. *Chem. Geol.* **2009**, *294*, 154-161.

(16) van Leeuwen, H. P.; Buffle, J. Chemodynamics of aquatic metal complexes: from small ligands to colloids. *Environ. Sci. Technol.* **2009**, *43*, 7175-7183.

(17) van Leeuwen, H. P.; Duval, J. F. L.; Pinheiro, J. P.; Blust, R.; Town, R. M. Chemodynamics and bioavailability of metal ion complexes with nanoparticles in aqueous media. *Environ. Sci.: Nano* **2017**, *4*, 2108-2133.

(18) van Leeuwen, H. P.; Buffle, J.; Duval, J. F. L.; Town, R. M. Understanding the extraordinary ionic reactivity of aqueous nanoparticles. *Langmuir* **2013**, *29*, 10297-10302.

(19) Duval, J. F. L.; Wilkinson, K. J.; van Leeuwen, H. P.; Buffle, J. Humic substances are soft and permeable: evidence from their electrophoretic mobilities. *Environ. Sci. Technol.* **2005**, *39*, 6435-6445.

(20) Ritchie, J. D.; Perdue, E. M. Proton-binding study of standard and reference fulvic acids, humic acids, and natural organic matter. *Geochim. Cosmochim. Acta*, **2003**, *67*, 85-96.

(21) Dinar, E.; Mentel, T. F.; Rudich, Y. The density of humic acids and humic like substances (HULIS) from fresh and aged wood burning and pollution aerosol particles. *Atmos. Chem. Phys.* **2006**, *6*, 5213-5224.

(22) Avena, M. J.; Vermeer, A. W. P.; Koopal, L. K. Volume and structure of humic acids studied by viscometry pH and electrolyte concentration effects. *Coll. Surf. A: Physicochem. Eng. Aspects* **1999**, *151*, 213-224.

(23) Reid, P. M.; Wilkinson, A. E.; Tipping, E.; Jones, M. N. Determination of molecular weights of humic substances by analytical (UV scanning) ultracentrifugation. *Geochim. Cosmochim. Acta* **1990**, *54*, 131-138.

(24) Duval, J. F. L. Electrokinetics of diffuse soft interfaces. 2. Analysis based on the nonlinear Poisson-Boltzmann equation. *Langmuir* **2005**, *21*, 3247-3258.

(25) Ohshima, H.; Kondo, T. Relationship among the surface potential, Donnan potential and charge density of ion-penetrable membranes. *Biophys. Chem.* **1990**, *38*, 117-122.

(26) Ohshima, H. Donnan potential and surface potential of a spherical soft particle in an electrolyte solution. *J. Coll. Interf. Sci.* **2008**, *323*, 92-97.

(27) van Leeuwen, H. P.; Town, R. M.; Buffle, J. Impact of ligand protonation on Eigen-type metal complexation kinetics in aqueous systems. *J. Phys; Chem. A* **2007**, *111*, 2115-2121.

(28) Polyakov, P.; Duval, J. F. L. Speciation dynamics of metals in dispersion of nanoparticles with discrete distribution of charged binding sites. *Phys. Chem. Chem. Phys.* **2014**, *16*, 1999-2010.

(29) Moussa, M.; Caillet, C.; Town, R. M.; Duval, J. F. L. Remarkable electrokinetic features of charge-stratified soft nanoparticles: mobility reversal in monovalent aqueous electrolyte. *Langmuir* **2015**, *31*, 5656-5666.

(30) Duval, J. F. L.; Town, R. M.; van Leeuwen, H. P. Poisson-Boltzmann electrostatics and ionic partition equilibration of charged nanoparticles in aqueous media. *J. Phys. Chem. C.* **2018**, *122*, 17328-17337.

(31) Manning, G. S. Limiting laws and counterion condensation in polyelectrolyte solutions. IV. The approach to the limit and the extraordinary stability of the charge fraction. *Biophys. Chem.* **1977**, *7*, 95-102.

(32) Town, R. M.; van Leeuwen, H. P. Intraparticulate metal speciation analysis of soft complexing nanoparticles. The intrinsic chemical heterogeneity of metal-humic acid complexes. *J. Phys. Chem. A* **2016**, *120*, 8637-8644.

(33) Buffle, J.; Deladoey, P.; Greter, F. L.; Haerdi, W. Study of the complex formation of copper(II) by humic and fulvic substances. *Anal. Chim. Acta* **1980**, *116*, 255-274.

(34) Aiken, G. R.; Malcolm, R. L. Molecular weight of aquatic fulvic acids by vapor pressure osmometry. *Geochim. Cosmochim. Acta* **1987**, *51*, 2177-2184.

(35) Rostad, C. E.; Leenheer, J. A. 2004. Factors that affect molecular weight distribution of Suwannee river fulvic acid as determined by electrospray ionization/mass spectrometry. *Anal. Chim. Acta* **2004**, *523*, 269-278.

(36) Guéguen, C.; Cuss, C. W. Characterization of aquatic dissolved organic matter by asymmetrical flow field-flow fractionation coupled to UV-Visible diode array and excitation emission matrix fluorescence. *J. Chromatogr. A* **2011**, *1218*, 4188-4198.

(37) Galceran, J.; Companys, E.; Puy, J.; Cecília, J.; Garcés, J. L. AGNES: a new electroanalytical technique for measuring free metal ion concentration. *J. Electroanal. Chem.* **2004**, *566*, 95-109.

(38) Town, R. M.; van Leeuwen, H. P. Dynamic speciation analysis of heterogeneous metal complexes with natural ligands by stripping chronopotentiometry at scanned deposition potential. *Aust. J. Chem.* **2004**, *57*, 983-992.

(39) van Leeuwen, H.P.; Town, R. M. Electrochemical metal speciation analysis of chemically heterogeneous samples: the outstanding features of stripping chronopotentiometry at scanned deposition potential. *Environ. Sci. Technol.* **2003**, *37*, 3945-3952.

(40) Town, R. M.; van Leeuwen, H. P. Depletive stripping chronopotentiometry: a major step forward in electrochemical stripping techniques for metal ion speciation analysis. *Electroanalysis* **2004**, *16*, 458-471.

(41) Town, R. M.; van Leeuwen, H. P. Fundamental features of metal ion determination by stripping chronopotentiometry. *J. Electroanal. Chem.* **2001**, *509*, 58-65.

(42) Town, R. M.; van Leeuwen, H. P. Effects of adsorption in stripping chronopotentiometric metal speciation analysis. *J. Electroanal. Chem.* **2002**, *523*, 1-15.

(43) d'Orlyé, F.; Reiller, P. E. Contribution of capillary electrophoresis to an integrated vision of humic substances size and charge characterizations. *J. Colloid Interf. Sci.* **2012**, *368*, 231-240.

(44) van Leeuwen, H. P.; Buffle, J.; Town, R. M. Electric relaxation processes in chemodynamics of aqueous metal complexes: from simple ligands to soft nanoparticulate complexants. *Langmuir* **2012**, *28*, 227-234.

(45) Dempsey, B. A. *The Protonation, Calcium Complexation and Adsorption of a Fractionated Aquatic Fulvic Acid.* PhD thesis, University of North Carolina at Chapel Hill, 1981.

(46) Lu, Y.; Allen, H. E. Characterization of copper complexation with natural dissolved organic matter (DOM) – link to acidic moieties of DOM and competition by Ca and Mg. *Wat. Res.* **2002**, *36*, 5083-5101.

(47) Krishnan, K.; Plane, R. A. Raman spectra of ethylenediaminetetraacetic acid and its metal complexes. *J. Am. Chem. Soc.* **1968**, *90*, 3195-3200.

(48) Clapp, L. A.; Siddons, C. J.; Whitehead, J. R.; van Derveer, D. G.; Rogers, R. D.; Griffin, S. T.; Jones, S. B.; Hancock, R. D. Factors controlling metal-ion selectivity in the binding sites of calcium-binding proteins. The metal-binding properties of amide donors. A crystallographic and thermodynamic study. *Inorg. Chem.* **2005**, *44*, 8495-8502.

(49) Travers, C.; Marinsky, J A. The complexing of Ca(II), Co(II), and Zn(II) by polymethacrylic and polyacrylic acid. *J. Polym. Sci.* **1974**, *47*, 285-297.

(50) van Leeuwen, H. P.; Town, R. M. Electric condensation of divalent counterions by humic acid nanoparticles. *Environ. Chem.* **2016**, *13*, 76-83.

(51) Goto, T.; Ikehata, A.; Morisawa, Y.; Higashi, N.; Ozaki, Y. The effect of metal cations on the nature of the first electronic transition of liquid water as studied by attenuated total reflection far-ultraviolet spectroscopy. *Phys. Chem. Chem. Phys.* **2012**, *14*, 8097-8104.

(52) Tipping, E. Humic ion-binding model VI: an improved description of the interactions of protons and metal ions with humic substances. *Aquat. Geochem.* **1998**, *4*, 3-48.

(53) Kinniburgh, D. G.; van Riemsdijk, W. H.; Koopal, L. K.; Borkovec, M.; Benedetti, M.; Avena, M. J. Ion binding to natural organic matter: competition, heterogeneity, stoichiometry and thermodynamic consistency. *Coll. Surf. A.* **1999**, *151*, 147-166.

(54) Yasuda, M.; Yamasaki, K.; Ohtaki, H. Stability of complexes of several carboxylic acids formed with bivalent metals. *Bull.Chem.Soc.Jpn*. **1960**, *33*,1067-1070.

(55) Pinheiro, J. P.; Mota, A. M.; Gonçalves, M. L. S. Complexation study of humic acids with cadmium(II) and lead(II). *Anal. Chim. Acta* **1994**, *284*, 525-537.

(56) Turner, D. R.; Whitfield, M.; Dickson, A. G. The equilibrium speciation of dissolved components in freshwater and seawater at 25°C and 1 atm pressure. *Geochim. Cosmochim. Acta* **1981**, *45*, 855-881.

(57) Maizel, A. C.; Remucal, C. K. Molecular composition and photochemical reactivity of size-fractionated dissolved organic matter. *Environ. Sci. Technol.* **2017**, *51*, 2113-2123.

(58) Galindo, C.; Del Nero, M. Molecular level description of the sorptive fractionation of a fulvic acid on aluminium oxide using electrospray ionization Fourier transform mass spectrometry. *Environ. Sci. Technol.* **2014**, *48*, 7401-7408.

(59) Schulten, H.-R.; Leinweber, P. Characterization of humic and soil particles by analytical pyrolysis and computer modeling. *J. Anal. Appl. Pyrol.* **1996**, *38*, 1-53.

(60) Buffle, J.; Altmann, R. S.; Filella, M. Effect of physico-chemical heterogeneity of natural complexants. Part II. Buffering action and role of their background sites. *Anal. Chim. Acta* **1990**, *232*, 225-237.

(61) Buffle, J.; Altmann, R. S.; Filella, M.; Tessier, A. Complexation by natural heterogeneous compounds: site occupation distribution functions, a normalized description of metal complexation. *Geochim. Cosmochim. Acta* **1990**, *54*, 1535-1553.

(62) Town, R. M.; Filella, M. Dispelling the myths: is the existence of L1 and L2 ligands necessary to explain metal ion speciation in natural waters? *Limnol. Oceanogr.* **2000**, *45*, 1341-1357.

TABLE OF CONTENTS ART

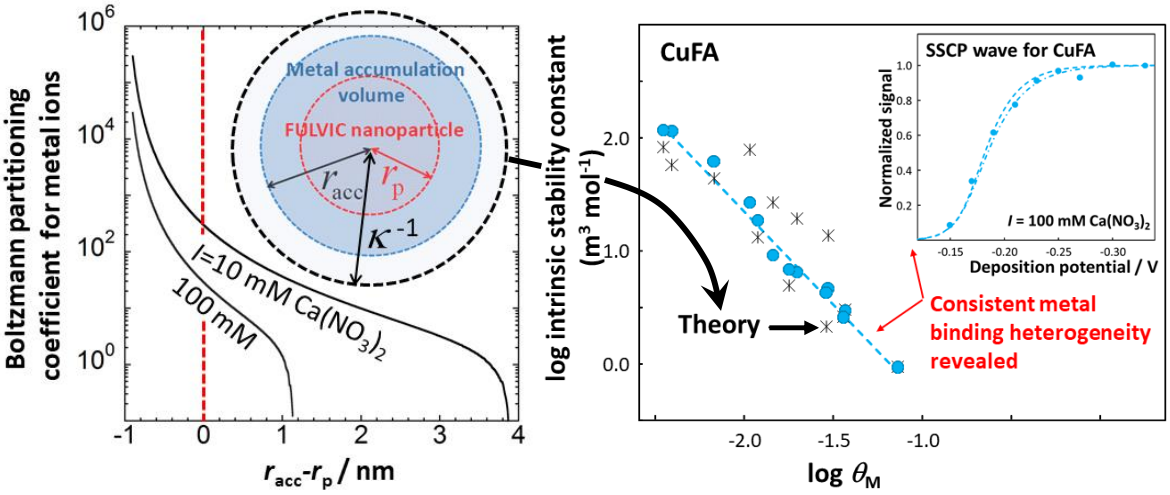

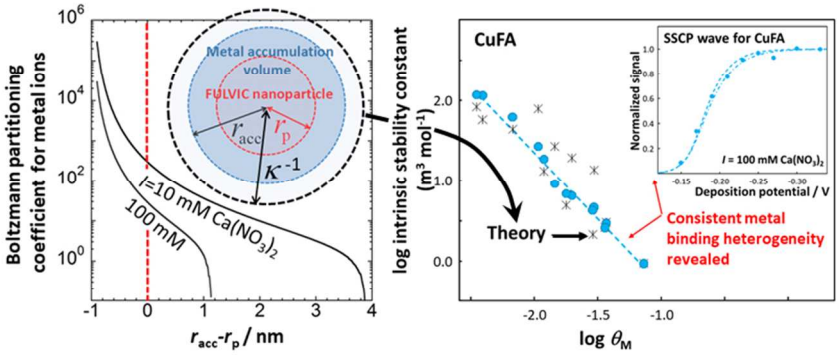

254x190mm (96 x 96 DPI)